

Development and Experimental Analysis of a Soft Compliant Tactile Microsensor for Anthropomorphic Artificial Hand

Lucia Beccai, *Member, IEEE*, Stefano Roccella, Luca Ascari, *Member, IEEE*, Pietro Valdastri, *Member, IEEE*, Arne Sieber, *Member, IEEE*, M. Chiara Carrozza, *Associate Member, IEEE*, and Paolo Dario, *Fellow, IEEE*

Abstract—This paper presents the development and preliminary experimental analysis of a soft compliant tactile microsensor (SCTM) with minimum thickness of 2 mm. A high shear sensitive 1.4 mm³ triaxial force microsensor was embedded in a soft, compliant, flexible packaging. The performance of the whole system, including the SCTM, an electronic hardware and a processing algorithm, was evaluated by static calibration, maximum load tests, noise and dynamic tests, and by focusing on slippage experiments. A proper tradeoff between final robustness and sensitivity of the tactile device was identified. The experiments showed that the tactile sensor is sufficiently robust for application in artificial hands while sensitive enough for slip event detection. The sensor signals were elaborated with the cumulative summation algorithm and the results showed that the SCTM system could detect a slip event with a delay from a minimum of 24.5 ms to a maximum of 44 ms in the majority of experiments fulfilling the neurophysiological requirement.

Index Terms—Artificial hand, microelectromechanical systems (MEMS) packaging, slippage detection, tactile microsensor.

I. INTRODUCTION

AMONG other functionalities (e.g., thermal sensing, nociception), the bioinspired tactile system must provide information about contact and slippage at the fingertip–object interface [1], and force and contact sensors are the minimal set of sensors suggested for the control of basic manipulation tasks [2]. In the artificial fingertips of anthropomorphic hands, it is important to mimic the distribution of sensory receptors. In particular,

Manuscript received October 3, 2006; revised July 2, 2007. Recommended by Technical Editor F. Karray. This work was supported in part by European Union (EU) under the NEUROscience and roBOTICS (NEUROBOTICS) Integrated Project (IST-FET Project 2003-001917) and in part by the Improving Human Potential (IHP) EU Programme in collaboration with the Institut fuer Mikrotechnik Mainz GmbH, Germany.

L. Beccai, S. Roccella, and M. C. Carrozza are with the Advanced Robotics Technology and Systems (ARTS) Laboratory, Scuola Superiore Sant'Anna, Pisa 56127, Italy (e-mail: lucia@arts.sssup.it; roccella@arts.sssup.it; carrozza@sssup.it).

P. Valdastri is with the Center of Research in Microengineering (CRIM) Laboratory, Scuola Superiore Sant'Anna, Pisa 56127, Italy (e-mail: valdastri@crim.sssup.it).

P. Dario is with the Advanced Robotics Technology and Systems (ARTS) Laboratory and Center of Research in Microengineering (CRIM) Laboratory, Scuola Superiore Sant'Anna, Pisa 56127, Italy (e-mail: dario@sssup.it).

L. Ascari is with the Advanced Robotics Technology and Systems (ARTS) Laboratory, Scuola Superiore Sant'Anna, Pisa 56127, Italy. He is now with HENESIS s. r. l., Parma 43100, Italy, and also with the Centre of Excellence for Information and Communication Engineering (CEIIC), Scuola Superiore Sant'Anna, Pisa 56127, Italy (e-mail: ascari@sssup.it).

A. Sieber is with Profactor Research and Solutions GmbH, Seibersdorf 2444, Austria (e-mail: arne.sieber@profactor.at).

Digital Object Identifier 10.1109/TMECH.2008.918483

by providing information about the distribution of both normal and shear components of the contact forces at the digit–object interface, together with their variation when slip events occur, contact conditions and object information could be gathered in detail and used to improve manipulation. In this framework, the research challenge is to implement sensory elements that can encode such bioinspired tactile information while fulfilling demanding technological and mechanical requirements. They need to be miniaturized and built with technological approaches that allow a distributed integration in the artificial fingers, while at the same time, they have to emulate the mechanical characteristics of the biological skin model. Sensors must have packaging endowing the final tactile system with characteristics like robustness, and at the same time flexibility, softness, and compliance without compromising the tactile sensitivity of the device. In particular, softness and compliance are essential in order to allow an artificial hand to interact properly with the environment and to perform stable grasps.

Numerous kinds of tactile sensors were proposed (for reviews, see [3] and [4]) and contact force sensing and slippage problems were addressed in many ways, and for the most part, with separate sensors that were integrated at the same time in artificial hands fingertips. Polyvinylidene Fluoride (PVDF), while not suitable to sense static contact, was mainly used for slip sensing due to its dynamic behavior, and in particular, for incipient slip identification [5], [6]. The PVDF needs to be coupled with other technologies in order to achieve contact force sensing. For example, in [7], this was achieved by combining in a robotic fingertip a PVDF strip with a pressure-variable resistor ink sensor, while earlier in [8], the PVDF strips were embedded on top of an 18 mm × 18 mm force sensor used to monitor the normal and shear force from a grasped object. The approach of combining different sensors was also introduced by Dario *et al.* [9] who developed a robot finger able to detect, in addition to temperature, the contact normal force (by force sensing resistors) and vibration using a piezoelectric ceramic bimorph. Moreover, thick film technology was used to develop and combine in a fingertip a piezoelectric sensor for slip sensing and piezoresistive strain sensors for static normal load measurements [10]. Recent research efforts in PVDF based tactile sensors were in measuring the magnitude and the position of the applied load also as well as the compliance of the contact object, as reported in [11] for minimally invasive procedures. Also, efforts were directed in achieving some distribution in a soft fingertip by embedding PVDF strips at different depths [12].

Microelectromechanical systems (MEMS) technology is a very powerful approach for building miniaturized devices that could be used for integration of smart and distributed tactile systems in artificial hands. Such technology offers the opportunity of developing high-reliability tactile sensors and sensor arrays, with small dimensions. The possibility of electronic integration makes the microsensors particularly attractive for the implementation of sensory arrays where the amount of data can be overwhelming and local signal processing of sensor signals is necessary. Nevertheless, not enough attention was paid on the identification of packaging strategies that could enable MEMS tactile sensors to be effectively used in artificial hands. MEMS sensors based on capacitive [13], [14] piezoresistive [15]–[17], and other sensor principles (also coupled, e.g., pneumatic and piezoresistive [18] and vacuum microelectronic [19]) were developed and several of them have implemented normal and shear force sensing. Shan *et al.* [20] report the fabrication of 4×4 MEMS array of 3-D force sensors (each larger than $4 \text{ mm} \times 4 \text{ mm}$) on a flexible printed circuit board (PCB) substrate. However, while detection of normal and shear forces was provided, the devices were still too bulky or lacked mechanical compliance and robustness, and the packaging of the systems was not developed. On the other hand, in cases in which softness and compliance were achieved, only pressure sensing or normal force sensing could be obtained. Also, it was not demonstrated how such devices could be used to detect slippage. In addition to silicon microstructuring, polymer micromachining has been applied in the field of tactile sensing [21]–[24]. A recent development [23] is that of a ground reaction force (GRF) sensor for a humanoid robot that achieved shear and normal load detection. The sensor was built from subsequent layers of finely structured polyimide, Cu–Ni metal strain gauges, and by exploiting an SU8 bump structure. The advantages of this technology are mainly the flexibility of the devices and low cost. Nevertheless, it cannot replicate the advantages of silicon sensing (e.g., the integration of sensory circuitry and keep wiring at a minimum level, the fabrication of 3-D fully integrated microstructures, etc.). Moreover, additional materials would still need to be identified and integrated on top of the polymer structured sensors, to confer to the devices the characteristics required to be interfaced properly with external objects. Also, slippage detection has not been conceived.

This paper presents the development and experimental analysis of a soft compliant tactile microsensors (SCTM). The final purpose of this research approach is to provide information about normal and shear contact forces and slippage with one tactile element, whose core component is a 3-D MEMS that can be integrated in anthropomorphic artificial hand. A high shear sensitive 1.4 mm^3 3-D silicon microsensors [25], [26] was embedded in a soft, compliant, and flexible packaging with minimum total thickness of 2 mm. The main aim of this study was to identify a proper packaging for the microsensors, that would allow the tactile sensor to be sufficiently robust for application in artificial hands, while sensitive enough to detect slip events.

The system composed by the SCTM, an electronic hardware and a processing algorithm, was evaluated at first by static calibration, maximum load tests, noise and dynamic tests. Secondly,

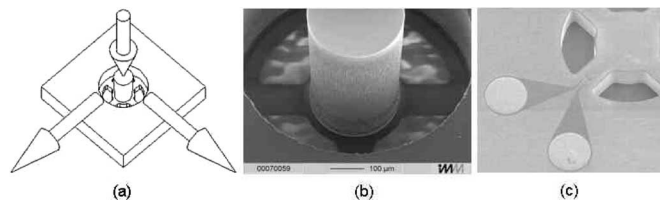


Fig. 1. (a) Sketch of the mechanical structure of the sensor where the normal and shear external applied forces are indicated. (b) SEM picture of the sensor showing the tethers (width $100 \mu\text{m}$) and central pillar ($\varnothing \sim 280 \mu\text{m}$). (c) SEM picture of sensor back side showing one piezoresistor connected by Al metals to two round Ni/Au bump pads ($\varnothing \sim 200 \mu\text{m}$).

slippage experiments were performed by exploiting an experimental setup that simulated the external stimuli that a grasped object would provide to the sensor when integrated in an artificial hand. The experimental analysis was focused on the transient phenomena when a change of static to dynamic friction condition occurred at the tactile microsensors surface, during interaction with an external object with different roughness, and sensor signals were elaborated by means of the cumulative summation algorithm. The scientific results of this paper are important to assess the bioinspired design methodology aimed at obtaining sensor specifications and performance as similar as possible to the natural model represented by the neurophysiology of grasping and manipulation [27]–[29].

The paper is organized as follows. The development of the SCTM is presented in Section II-A. The experimental apparatus is reported in Section II-B, while Section II-C is dedicated to the description of the protocol of the experimental analysis that was performed by means of static calibration and maximum load tests, noise, dynamic behavior, and slippage experiments. The applied signal processing approach is explained in Section II-D. The experimental results are described in Section-III, while in Section IV, the discussion and conclusions are reported.

II. MATERIALS AND METHODS

A. Development of the Soft Compliant Tactile Microsensor

The triaxial force microsensors, representing the core component of the device presented in this paper, was earlier reported for its design, fabrication, and characterization [25], [26]. Briefly, the silicon sensor ($1.5 \text{ mm} \times 1.5 \text{ mm} \times 625 \mu\text{m}$) has a high aspect ratio structure with an integrated silicon mesa used for the transmission of the force to a flexible tethered structure, where four integrated piezoresistors are used independently to detect the three components of an external applied force. A sketch of the mechanical structure of the sensor where the normal and shear external applied forces are indicated is represented in Fig. 1(a). The external load is transferred to the cylindrical mesa of the sensor at one side (See Fig. 1(b)), whereas the electrical connections must be performed at the opposite side of the sensible structure. Piezoresistors and their contacts are integrated in the flexible tethers and sensor bulk, respectively, as shown in Fig. 1(c). The sensor can be bonded to a silicon carrier chip, as reported in [25], and it must be packaged with flexible connections in order to develop a smart skin.

The microsensor has a hybrid microsystem architecture that allows independent optimization of the technology and specifications for the sensor part, packaging, and electronic circuitry. Envisaging a support chip in the microsystem design is very important for future integration of electronics and local sensor signal processing that could be done without the need to change any step in the technological process of the sensor itself. In this study, only the sensor part was employed in order to investigate its response with the proposed packaging, taking care that the packaging procedure and materials are also suitable for future integration of the silicon support chip.

1) *Packaging of the Microsensor*: The packaging of the microsensor consisted of two main phases, i.e., the bonding of the microsensor to flexible connections and the integration of a mechanical interface between the microsensor and the outer world that protects the sensor and through which external actions need to be detected by the sensor itself.

Flexible connections were obtained from LF9150R Pyralux (DuPont, Wilmington, DE) consisting of a 127- μm -thick Kapton sheet with a 35- μm layer of copper (Cu) (305 g/m^2) on one side. The Cu layer was patterned by photolithography using a MicroPosit S1813 photoresist (Shipley, USA) and 100- μm Cu metals could be obtained.

The layout of the microsensor includes nine Ni/Au round bump pads ($\text{Ø } 200 \mu\text{m}$) shown in Fig. 1(c). They were designed with dimensions compatible with the polymer flip-chip bonding technique that was previously employed to bond the sensor to a carrier substrate [25]. In this paper, the sensor contacts were bonded directly to corresponding copper pads on the Kapton substrate. A proper bonding technique between the microsensor and the flexible circuit was identified in order to establish mechanically and electrically reliable contacts. The 5552 R Z-Axis Adhesive Film (3M, St. Paul, MN) was exploited for mounting the sensor on the flexible circuit. This component is a heat-bonded, electrically anisotropic conductive film consisting of an adhesive matrix randomly loaded with conductive particles. These particles allowed electrical connection through the film thickness (vertical axis), but were spaced far enough from each other to avoid electrical connections in the horizontal plane. The main advantage in using such adhesive film is that serial bonding of each pad could be avoided. A microassembly station was set up which allowed both the alignment of the sensor on the flexible circuit and the control of the curing parameters, i.e., pressure (20–40 kg/cm^2) and temperature (170 $^\circ\text{C}$). Reliable and strong mechanical bondings (sensor detachment from the flexible circuit was unsuccessful without breaking the sensor bulk) were achieved, and electrical contacts had resistances below 1 Ω .

After mounting the microsensor on the flexible circuit, as described earlier, the next step toward the final tactile sensor prototype was the encapsulation in a soft and compliant material.

In the complex process of identification of proper sensor packaging materials that could be considered for attempting emulation of the compliance and friction properties of the natural human finger, some fundamental technological and mechanical type of requirements need to be fulfilled. The materials must ensure protection to the sensor structure while not impairing its function, thus allowing a proper tradeoff between

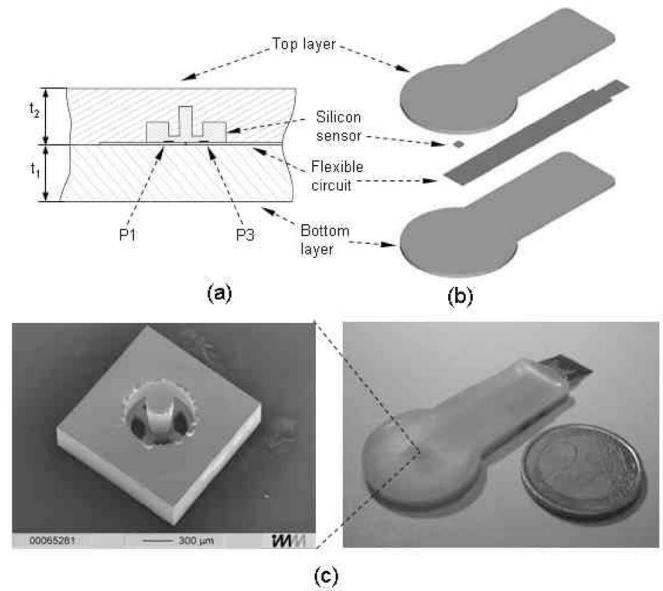


Fig. 2. Packaging components of the SCTM prototype in (a) 2-D section showing the position of two of the integrated piezoresistors, called P1 and P3, and in (b) an exploded display; (c) on the right, picture depicting the packaged prototype (with $t_1 = t_2 = 1 \text{ mm}$) with indicated the area ($\text{Ø } \sim 3 \text{ mm}$) where the microsensor (shown on the left) is embedded.

final robustness and sensitivity of the tactile device. In addition, the curing parameters of the chosen material must be compatible with the physical and technological characteristics of the sensor.

In this paper, in order to address the aforementioned basic requirements, the selected materials for the microsensor packaging were silicone and polyurethane. First, trials were performed using polydimethylsiloxane PDMS silicone elastomer (Sylgard 184, Dow Corning). Nevertheless, silicone typically has very low adhesion to nonsilicone materials. Also, during the curing phase, shrinkage of the material occurred. These effects lead to an empty space left in between the microsensor surface and the cured silicone used for packaging, introducing undesired hysteresis effects. In a second phase, the material used for the microsensor packaging was the two components soft polyurethane Poly 74–45 (PolyTek, USA), which adhered well to the MEMS device and embedded it by penetrating into the empty cavities of the microsensor. The easier flowing of the polyurethane material around the 3-D structure of the microsensor, with respect to the silicone elastomer applied in earlier trials, was also due to the lower viscosity (2500 mPa of the Poly 74–45 versus 5500 mPa of the Sylgard 184). Importantly, studies on such type of polyurethane material, as regards the conformance characteristics with respect to the human fingertip skin, suggested that it could be considered for the artificial emulation of the epidermis/dermis layer [30].

As described in the Section II-B, the shape and dimensions of the polyurethane packaging were designed in order to allow proper alignment of the prototype and the experimental apparatus used for testing. As shown in Fig. 2, the round-shaped part of the prototype had larger dimensions ($\text{Ø } 25 \text{ mm}$) than those of

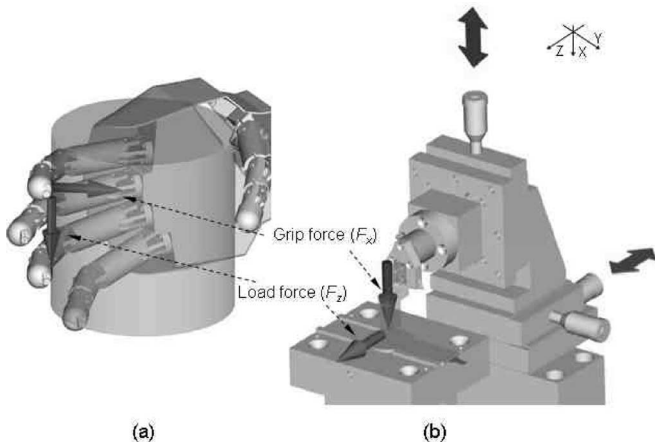


Fig. 3. (a) Grip and load forces occurring at the fingertip–object interface during grasping activities. (b) Same forces produced by means of the experimental apparatus and imposed to the SCTM.

the packaged sensor ($\varnothing \sim 3$ mm). A Teflon mould was built in order to achieve the proper shape of the package.

The encapsulation process consisted of several steps. At first, a layer of polyurethane [having thickness $t_1 = 1$ mm as shown in Fig. 2(a)] was poured into the mould that was subsequently put into a vacuum oven to remove air bubbles. The curing phase was performed at 100°C for 1 h. Once the first polyurethane layer was cured, the MEMS sensor and the connected flexible circuit were placed on top of the polyurethane film, as represented in Fig. 2. A second layer of polyurethane was poured on the device to achieve the encapsulation at the desired thickness $t_2 = 1$ mm [as indicated in Fig. 2(a)]. Polymerization of the soft material was obtained with the same curing procedure applied for the first layer. Fig. 2 shows the schematic model and a picture of the resulting Soft Compliant Tactile Microsensor that will be addressed as SCTM in the following sections.

B. Experimental Apparatus

As schematically represented in Fig. 3(a), the contact forces occurring at finger–object interface during grasping activities can be resolved in normal and tangential components relative to the plane tangential to the contact surface. The normal component is the grip force and the tangential component in the vertical direction is the load force. The moment at which a grasped object starts to slide corresponds to the change of static to dynamic friction condition.

The SCTM experimental analysis was focused on slippage experiments and the experimental apparatus was purposely conceived in order to emulate the sliding event due to a change of the grasped object weight. As schematically shown in Fig. 3(b), the probe was pressed against the surface of the prototype in the normal direction (x -axis), mimicking the grip force (F_x), and a sliding movement was imposed to the probe along the tangential direction (z -axis), simulating a variable load force (F_z).

The experimental apparatus consisted of three main modules, as schematically illustrated in Fig. 4(a) and depicted in Fig. 4(b): the loading system, the SCTM mounted on a

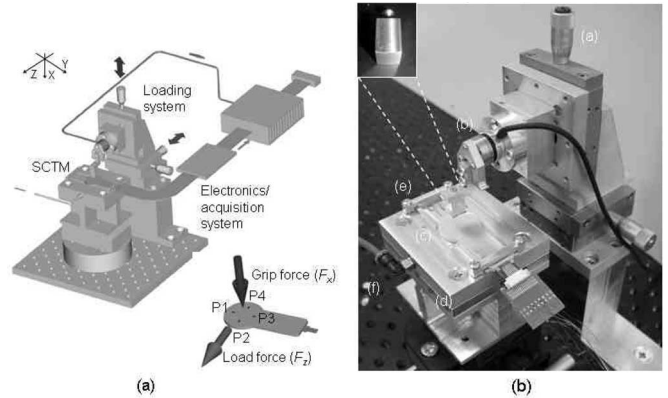


Fig. 4. (a) Schematic display of the experimental apparatus. The inset shows the four SCTM piezoresistors (indicated as P1, P2, P3, and P4) alignment with respect to the applied grip and load forces. (b) Global view of the experimental apparatus. An enlarged view of the loading probe is depicted in the inset.

fixture, and the electronics/acquisition system. The loading system exploited three micrometric translation stages with crossed roller bearing (a) (M-105.10, PI, Karlsruhe, Germany), that allowed the positioning of the loading structure on the sensor under test. Load was applied to the sensor through a six components load cell (b) (ATI NANO 17 F/T, Apex, NC) interfaced to the x -axis translation stage. The load was applied to the sensor by means of a probe consisting of an aluminium block (dimensions $9\text{ mm} \times 6.55\text{ mm} \times 15\text{ mm}$) with a curved contact surface (curvature radius of 30 mm). The probe was chosen to represent common cylindrical objects that are manipulated during daily living activities. Tests were performed by using both the aluminium probe contact surface and the same probe covered with sandpaper grade P400. The SCTM (c) was constrained to the fixture (d) both mechanically (e) and by means of an air suction system (f), in order to guarantee its stable position during the sliding experiments. The outer shape of the microsensor packaging had a round part (as shown in Fig. 2) that was used to produce a proper alignment of the SCTM and the loading system. The design approach followed for both the mechanical support structure and the loading system, allowed the alignment between the probe and the support axes. When the prototype under test was fixed, the axis of its round shape coincided with the axis of the mechanical support (d). Thus, as final result, the prototype and probe axes were aligned.

The signal conditioning electronics were designed in order to obtain an output voltage proportional to the fractional change in resistance $\Delta R/R$. Each resistor, typically ranging from $800\ \Omega$ to $1\text{ k}\Omega$ was independently conditioned, using a quarter Wheatstone bridge configuration with two precision $1\text{ k}\Omega$ resistors and one trimmer, in order to remove the initial offset level. The bridge output signals were then amplified to $\pm 10\text{ V}$ range by four instrumentation amplifier (AD620, Analog Devices, Norwood, MA) with a gain of 430. The power consumption obtained using the signal conditioning circuit was about 10 mW per sensor. A more sophisticated circuitry can be designed in order to further decrease the power consumption of the sensor.

No analog filtering was applied to the signals. A National Instruments Data Acquisition Card (NI-PCI-6034E) digitized the four signals with 16 bit resolution, meaning 0.3 mV. The software platform used was Windows XP and National Instruments Laboratory View 7 Express.

C. Experimental Protocol

Previous to slippage experiments, a set of preliminary tests were planned and performed. They consisted of static calibration, maximum load tests, noise and dynamic tests.

The static calibration was performed by applying increasing static normal and tangential loads by means of the experimental apparatus depicted in Fig. 4. Maximum load tests were performed to verify the SCTM robustness by applying maximum normal and tangential loads of 15 and 11 N, respectively. Those were the maximum values allowable with the ATI load cell.

After assessing the static behavior of the SCTM, the noise and dynamic behavior were tested. Noise analysis was performed by acquiring the SCTM response at applied static normal loads of 0, 1, and 2.5 N. The electronics and acquisition system described in Section II-B was used to sample the outputs of the sensor at 50 kHz. The power spectrum of the noise, its time distribution, and rms value were computed. Dynamic loading tests were performed to verify the SCTM capability to detect the variations of the applied loads between dc and 400 Hz, which is the bandwidth that emulates the dynamic behavior of all human mechanoreceptors [31]. The SCTM dynamic behavior was investigated by using the same apparatus shown in Fig. 4. A steel sphere (\varnothing 6 mm) was dropped on the sensor in order to provide an impulsive stimulus and to excite all the vibration modes of the structure. The corresponding output signals were analyzed to extract the power spectral density.

Following the set of experimental tests described earlier, the experimental protocol for the study on slippage detection was applied. The probe of the loading system was manually aligned with respect to the SCTM prototype. The probe was pressed on the prototype in the normal direction (x -axis) with a normal force F_x lower than the loads measured during maximum load tests. A ramp displacement of 15 mm was imposed to the probe by means of the z -axis translation stage. A total of 15 experiments were performed by means of the aluminium probe and with the sandpaper one.

The inset of Fig. 4(a) schematically shows the position of the four piezoresistors, indicated as P1, P2, P3, and P4, of the SCTM with respect to the applied grip and load forces. The direction of the sliding movement was mainly from P4 toward P2. This was due to the packaging procedure that did not guarantee a perfect alignment of the sensor silicon tethers (and piezoresistors) axis with respect to the z and y -axes of the experimental apparatus. Nevertheless, such misalignment was accepted in the framework of this study because, as described in the following Sections-II-D and III-B, the slippage detection strategy was based on the estimation of the friction cone that involves all the components of the contact force vector at the interface between the probe and the SCTM prototype.

D. Slippage Detection Process

At the instant of slip phenomena, a sudden change of the static friction coefficient μ_S to the dynamic friction coefficient μ_D occurs. Such coefficients were estimated by both the reference load cell and the SCTM. The Cumulative summation approach [32] was applied in the analysis of the SCTM signals in order to identify the moment in which a sudden change of the estimated friction coefficients occurred. The cumulative summation represents a good compromise between low computational requirements, performance, and robustness to noisy signals from one side, and accuracy and latency from the other. The algorithm, which can be tailored to the application requirements, is conceptually simple and could be efficiently implemented in commercial low profile microcontrollers allowing its integration in the final bio inspired tactile system in an artificial hand.

The SCTM signals were analyzed over a sliding window of k subsequent samples. Indicating by $x(i)$ ($i = 1, \dots, k$) the values of the samples of the signal inside the window, and by m their average, the cumulative sum at time $n \leq k$ is

$$S_n = \sum_{i=1}^n x(i) - m. \quad (1)$$

At each time interval, the value of M_n [as defined in (2)] inside the window is updated

$$M_n = \max_{0 \leq k \leq n} (S_k). \quad (2)$$

A negative jump is detected if and when

$$M_n - S_n \geq B \quad (3)$$

where the boundary B is proportional to the minimum amplitude of the jumps that the algorithm is detecting. By increasing B , the delay in the detection increases, as well as the robustness to spurious jumps. On the other side, by increasing k , the sensitivity of the algorithm to smaller jumps increases as well. The choice of k and B values optimized the recognition of the slip events. Both of them had to be chosen based on several constraints, like the noise characteristics of the signals being analyzed, as well as the minimum amplitude of the jumps to be detected. Moreover, the ratio μ_S/μ_D was estimated in order to tune the detecting algorithm parameters as reported in [33].

III. EXPERIMENTAL RESULTS

A. Static Calibration and Maximum Load Tests

The static calibration tests were performed in order to identify the relation between the external applied loads and the SCTM output signals for the estimation of the friction cone that is described in Section III-B.

Given V_1 , V_2 , V_3 , and V_4 the signals recorded from the four piezoresistors of the SCTM, V_{sum} , V_{13} , and V_{24} , are defined as follows:

$$V_{\text{sum}} = V_1 + V_2 + V_3 + V_4 \quad (4)$$

$$V_{13} = V_1 - V_3 \quad (5)$$

$$V_{24} = V_2 - V_4 \quad (6)$$

TABLE I
AVERAGE VALUES AND STANDARD DEVIATIONS OF THE LINEAR REGRESSION COEFFICIENTS (R^2) OF THE RELATIONSHIP BETWEEN F_z (GRIP FORCE) AND V_{24} , F_y AND V_{13} , F_x (LOAD FORCE) AND V_{sum} ARE REPORTED

	V_{24} vs. F_z (R^2)	V_{13} vs. F_y (R^2)	V_{sum} vs. F_x (R^2)
Avg	0.94	0.81	0.73
Stds	0.05	0.14	0.14

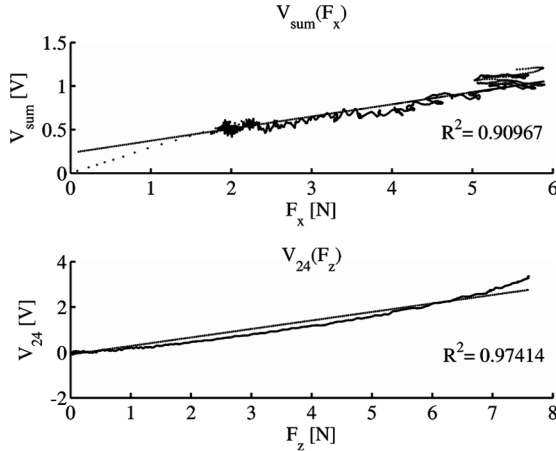


Fig. 5. Graphs showing the relationship between F_x and V_{sum} and F_z and V_{24} , relative to one static calibration experiment (n.2 as from Table IV in the Appendix).

The results of the calibration procedure showed a quite linear relationship between F_x and V_{sum} , F_y and V_{13} , and F_z and V_{24} . The average values and standard deviation of the linear regression coefficients (R^2), relative to all the experiments performed with the two different types of probe on the SCTM, are reported in Table I, while the R^2 values for each experiment are reported in the Appendix (Table IV).

The direction of the sliding movement during the slippage experiments was from P2 to P4 [see Fig. 4(A), inset], thus V_{13} showed near null values confirming a quite good alignment of the loading probe with the SCTM specimen. Therefore, in Fig. 5, the graphs relative to the results of one experiment are reported not representing V_{13} .

The SCTM robustness for the range of loads used during the slippage experiments was demonstrated since the prototypes did not break as a result of applying the maximum static loads of 15 and 11 N in the normal and tangential direction, respectively, for five trials. The load cell used in the experimental apparatus could not sustain higher loads necessary to verify the effective breaking loads of the SCTM.

B. Noise and Dynamic Behavior

The signals recorded during the experiments showed a high repeatability. The pronounced flatness of the noise power spectrum over the whole frequency range allowed to adopt the rms value as a good estimator of the noise level. In all the performed experiments, the noise rms was equal to 29.9 ± 2.9 mV. As regards to the SCTM dynamic behavior, the power spectrum showed a low-pass shape, with a cutoff frequency of 1.2 kHz

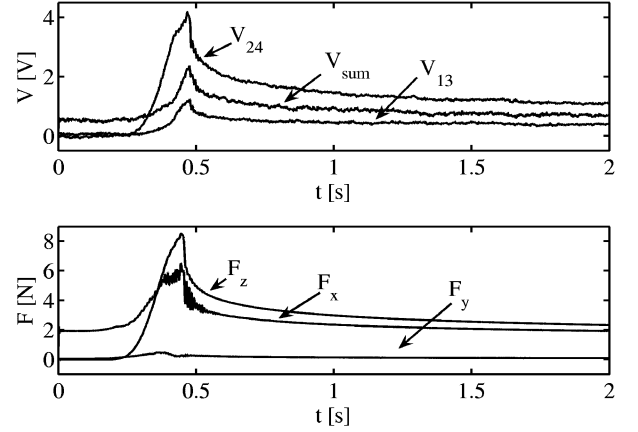


Fig. 6. Results of a slippage experiment performed with the Al probe on the SCTM. Top: the sum and difference of the SCTM voltage outputs V_{sum} , V_{13} , and V_{24} , respectively. Bottom: the forces of the reference load cell F_x , F_y , and F_z .

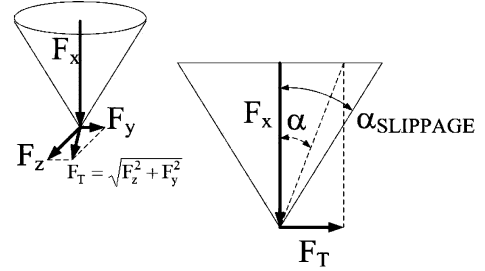


Fig. 7. Friction cone at the contact point between the probe and the SCTM.

and the response was nearly flat between dc and the cutoff frequency.

C. Slippage

The four output signals of the SCTM and the three force signals of the load cell, during a typical test employing the aluminium probe, are shown in Fig. 6.

Initially, a grip force (F_x) of 1.9 N was imposed to the SCTM. At time $t \approx 0.3$ s, the probe sliding movement (from P2 to P4 as shown in Fig. 4) started. In the time interval of 0.3–0.46 s, there was static friction at the interface between the probe and the SCTM. During the same time interval, the load force (F_z) increased significantly, reaching a maximum at approximately $t = 0.46$ s, when a sudden change in all the recorded load cell signals occurred detecting the slip event. The SCTM output signals showed a sudden change as well. From this moment, there was a mechanical sliding between the probe and the SCTM, and friction changed from static to dynamic condition.

Considering the friction cone at the contact point between the probe and the SCTM, as shown in Fig. 7, the static and dynamic friction coefficients, μ_S and μ_D , are defined as

$$\begin{aligned} \mu_S &= \tan(\alpha_{slippage}) = \frac{|F_T|_{slippage}}{|F_X|_{slippage}} \\ &= \frac{\sqrt{|F_Z|_{slippage}^2 + |F_Y|_{slippage}^2}}{|F_X|_{slippage}} = \text{Cone } F_{slippage} \end{aligned} \quad (7)$$

TABLE II
AVERAGE VALUES AND STANDARD DEVIATIONS OF γ ARE REPORTED FOR BOTH LOAD CELL AND SCTM

Al probe	γ_{SCTM}	$\gamma_{load\ cell}$
Avg	1.58	1.32
Stds	0.09	0.057
Sandpaper probe	γ_{SCTM}	$\gamma_{load\ cell}$
Avg	1.64	1.55
Stds	0.34	0.058

$$\mu_D = \tan(\alpha_\infty) = \frac{|F_T|_\infty}{|F_X|_\infty} = \frac{\sqrt{|F_Z|_\infty^2 + |F_Y|_\infty^2}}{|F_X|_\infty} = \text{Cone } F_\infty. \quad (8)$$

The ratio of the friction coefficients can be defined as

$$\gamma = \frac{\mu_S}{\mu_D} = \frac{\text{Cone } F_{\text{slippage}}}{\text{Cone } F_\infty} = \gamma_{\text{loadcell}} \quad (9)$$

where α_{slippage} is the angle of the friction cone, $|F_T|_{\text{slippage}}$ is the magnitude of the resultant of the tangential forces, $|F_X|_{\text{slippage}}$ is the magnitude of the normal force at the instant of the slip event, α_∞ is the angle of the friction cone, $|F_T|_\infty$ is the magnitude of the resultant of the tangential forces, and $|F_X|_\infty$ is the magnitude of the normal force at the end of the slippage experiment.

Given the linear relationship between the forces measured by the load cell and the SCTM output signals that was demonstrated during the static calibration experiments (Section III-A), it follows that

$$\mu_S \propto \frac{\sqrt{|V_{24}|_{\text{slippage}}^2 + |V_{13}|_{\text{slippage}}^2}}{|V_{\text{sum}}|_{\text{slippage}}} = \text{Cone } V_{\text{slippage}} \quad (10)$$

$$\mu_D \propto \frac{\sqrt{|V_{24}|_\infty^2 + |V_{13}|_\infty^2}}{|V_{\text{sum}}|_\infty} = \text{Cone } V_\infty. \quad (11)$$

As consequence of (9), (10), and (11),

$$\gamma = \frac{\mu_S}{\mu_D} \propto \frac{\text{Cone } V_{\text{slippage}}}{\text{Cone } V_\infty} = \gamma_{SCTM}. \quad (12)$$

In the analysis of the results of the slippage experiments, the γ values for the load cell and the SCTM, as defined in the equations earlier, were considered. In Table II, the average values and standard deviations of γ are reported, while the γ values for each experiment are reported in the Appendix (Table V).

The slip event was identified by the sudden transition from the static condition (Cone F_{slippage}) to the dynamic condition (Cone F_∞), thus the load cell was used in the experiments as the reference system. The noise rms affecting the load cell was two orders of magnitude lower than the one affecting the SCTM, thus the algorithm applied to the load cell produced a latency lower than 1 ms in slip event identification.

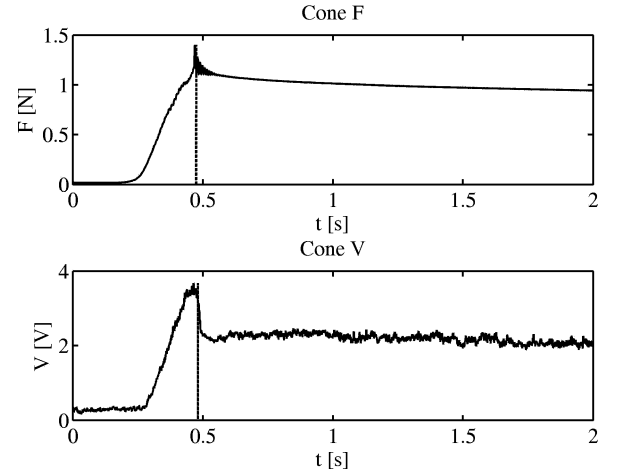


Fig. 8. Estimation of the friction cones relative to both the load cell and the SCTM system, corresponding to an experiment (n.3 as from Table III) performed with the aluminium probe.

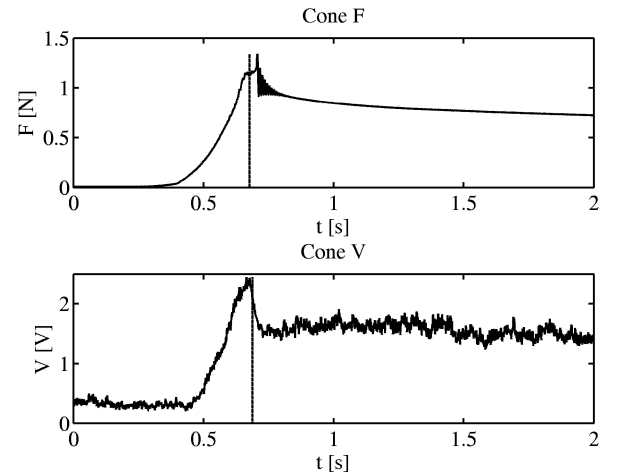


Fig. 9. Estimation of the friction cones relative to both the load cell and the SCTM system, corresponding to an experiment (n.15 as from Table III) performed with the probe covered with sandpaper.

Figs. 8 and 9 show the estimation of the friction cones relative to both the load cell and the SCTM system, corresponding to two slippage experiments. The output of the slip detection algorithm is indicated by the vertical line on the same time scale, showing that the SCTM system could detect slip events with certain delays with respect to the load cell system.

The delay with which the SCTM detected a slip event depended on the intrinsic properties of the tactile sensor itself, on the electronic hardware, and on the latency of the applied algorithm itself.

In Table III, the results of the experiments performed are shown, where t_{loadcell} and t_{SCTM} represent the time at which the slip event is detected by the load cell system and by the SCTM system, respectively, while t_D is the delay in slippage detection of the SCTM system with respect to the load cell.

Fig. 10 represents an enlarged view of the signals shown in Fig. 8 at the time frame correspondent to the slip event. In this experiment, the delay of the SCTM system in detecting slippage

TABLE III

RESULTS OF THE SLIPPAGE EXPERIMENTS ARE REPORTED: $t_{load\ cell}$ AND t_{SCTM} REPRESENT THE TIME AT WHICH THE SLIP EVENT IS DETECTED BY THE LOAD CELL SYSTEM AND BY SCTM SYSTEM, RESPECTIVELY. t_D IS THE DELAY IN SLIPPAGE DETECTION OF THE SCTM SYSTEM WITH RESPECT TO THE LOAD CELL

	Experiment n.	$t_{loadcell}$ (s)	t_{SCTM} (s)	t_D (s)
Al probe	1	0.487	0.5141	0.0271
	2	0.4105	0.4283	0.0178
	3	0.474	0.48	0.006
	4	0.5553	0.5992	0.0439
	5	0.3781	0.4274	0.0493
	6	0.531	0.5695	0.0385
	7	0.1841	0.2206	0.0365
Sandpaper probe	8	0.4726	0.4741	0.0015
	9	0.4269	0.4447	0.0178
	10	0.7356	0.7425	0.0069
	11	0.6558	0.6705	0.0147
	12	0.6566	0.696	0.0394
	13	0.6785	0.6931	0.0146
	14	0.5076	0.5211	0.0135
	15	0.6733	0.6868	0.0135

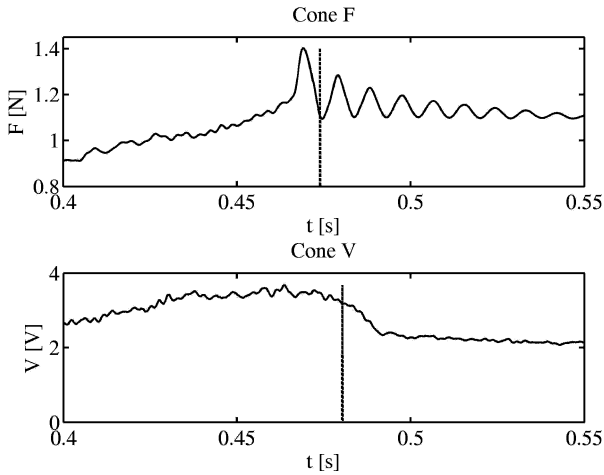


Fig. 10. Enlarged view of the same graph shown in Fig. 8., at the time frame correspondent to the slip event, in which the delay of the SCTM system in detecting slippage was of about 6 ms.

was about 6 ms. This result was obtained fixing the amplitude threshold B to four times the rms, and the window length $k = 90$ samples. These values, which proved to minimize on average the number of false positive and false negative detections, were used for all the experiments.

Fig. 11 shows the effect of varying B and k on the latency relative to the experiment of Fig. 10.

As discussed in [33], higher values of γ cause lower latency in the detection of jumps. This seems to be confirmed by the results of the experiments that showed a higher latency when using the aluminium probe with respect to the latency relative to experiments using sandpaper.

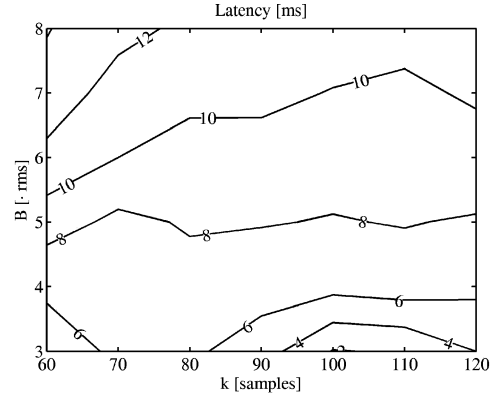


Fig. 11. Effect of B and k variations on SCTM latency relative to experiment shown in Fig. 10. The x -axis indicates the length of the sliding window in number of samples. The y -axis indicates the values of B (minimum amplitude of the jumps to be detected). The labels on the lines in the plot are the overall detection latencies in milliseconds.

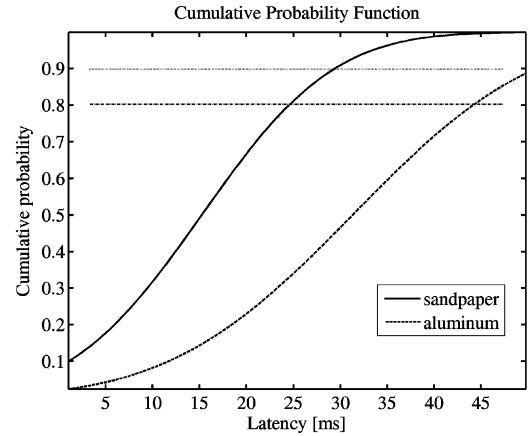


Fig. 12. Cumulative probability function of experiments with sandpaper covered prove (solid line) and aluminium probe (dashed line). The two horizontal lines correspond to 80% and 90% of the cases.

Fig. 12 shows the cumulative probability function of all the performed experiments with sandpaper and aluminium probes. In the 80% of the experiments performed with sandpaper, slippage was detected within 24.5 ms, while with aluminium, 44 ms were necessary. Considering a higher percentage of the experiments, i.e., 90%, the latencies increased to 29 and 52 ms, respectively. Experimental data were roughly normally distributed around 15.5 ms for sandpaper probe and 31.3 ms for aluminium.

IV. DISCUSSION AND CONCLUSION

In this paper, the development and preliminary experimental analysis of a soft compliant tactile microsensor (SCTM) was presented. A flexible, soft, compliant but robust packaging of a 1.4 mm^3 triaxial silicon microsensors was developed with minimum thickness of 2 mm. The performance of the whole system, including the SCTM, an electronic hardware, and a processing

algorithm was evaluated by static calibration, maximum load tests, noise and dynamic tests, and by focusing on slippage experiments.

The SCTM had a higher loading range with respect to the bare silicon microsensor that has a breaking normal and shear load of ~ 3 and ~ 0.5 N, respectively. The integration of soft, compliant and flexible materials by means of a purposely developed packaging process (reported in Section II-A) produced a tactile sensor that could withstand forces compatible to those involved in human fine grasping activities (i.e., about 4 N) [27]. The maximum measured values were of 15 and 11 N, for the normal and tangential static loads, respectively. Such values are in the range of the loads considered for the design of anthropomorphic artificial hands (i.e., 10 N) [1], [34]–[36].

At the same time, the scientific experiments performed by simulating object slippage demonstrated that the SCTM was intrinsically sensitive enough to detect a slip event.

The experiments were performed by using contact surfaces with different roughness (aluminium probe/SCTM, sandpaper probe/SCTM), and a dedicated processing algorithm was implemented in order to establish the instant of a slip event.

The slippage detection strategy was based on the estimation of the μ_S/μ_D ratio by means of the friction cone that involved all the components of the contact force vector at the interface between the probe (with which external loads are applied) and the SCTM prototype. This ratio was calculated for both the SCTM (γ_{SCTM}) and the reference load cell ($\gamma_{load\ cell}$) and the cumulative summation algorithm was applied to detect the instant of slippage in both systems. The experimental results showed a delay of the SCTM system with respect to the load cell.

According to a bioinspired approach, the biological response times to a slippage event must be taken into consideration in the analysis of the experimental results. Studies in neurophysiology demonstrated that the signals in tactile afferent units are used to adapt the grip:load force ratio during precision grip of an object to ensure grasp stability, and that the latency between the onset of slippage and the adjustment of such ratio is about 70 ms [27], [28]. From the statistical analysis, it resulted that in the 80% of the experiments, the SCTM system could detect a slip event with a delay that went from a minimum of 24.5 ms to a maximum of 44 ms. Among all the experiments performed, the minimum delay was of about 6 ms. All the delays were lower than the neurophysiological requirement; thus, the SCTM system approach could be considered for integration with an actuation and transmission system of an artificial hand, in order to investigate about the total system (including control) capability for slippage detection. The optimization of the electronic hardware could offer lower rms values to which the slippage detection algorithm latency is linked.

Future work will mainly consist on the optimization of the electronic system and on the integration of the SCTM in an anthropomorphic artificial hand, in order to effectively assess the capability to detect slip events during grasping and manipulation tasks.

APPENDIX

TABLE IV
LINEAR REGRESSION COEFFICIENTS (R^2) OF THE RELATIONSHIP BETWEEN F_z (GRIP FORCE) AND V_{24} , F_y AND V_{13} , F_x (LOAD FORCE) AND V_{sum} ARE REPORTED FOR EACH EXPERIMENT

	Experiment n.	V_{24} vs. F_z (R^2)	V_{13} vs. F_y (R^2)	V_{sum} vs. F_x (R^2)
Al probe	1	0.82094	0.92314	0.78235
	2	0.97414	0.83921	0.90967
	3	0.95585	0.9425	0.80352
	4	0.97456	0.92636	0.9372
	5	0.82035	0.92482	0.69426
	6	0.97039	0.89653	0.90287
	7	0.96223	0.95492	0.74785
Sandpaper probe	8	0.97656	0.87115	0.83205
	9	0.94629	0.739	0.77421
	10	0.96967	0.52996	0.49136
	11	0.95642	0.80392	0.59802
	12	0.8673	0.86311	0.55353
	13	0.95941	0.62071	0.63957
	14	0.95666	0.64465	0.58068
	15	0.97642	0.62772	0.70004
	Avg	0.939146	0.80718	0.729812
	Stds	0.054968	0.139581	0.137344

TABLE V
VALUES OF γ ARE REPORTED FOR BOTH LOAD CELL AND SCTM, FOR EACH EXPERIMENT

Probe type	Experiment n.	γ_{SCTM}	$\gamma_{load\ cell}$
Al probe	1	1.5024	1.2446
	2	1.7164	1.2584
	3	1.6967	1.3598
	4	1.4951	1.4116
	5	1.569	1.3247
	6	1.5308	1.308
	7	1.5634	1.3199
	Avg	1.5819	1.3181
	Stds	0.0896	0.0571
	Sandpaper probe	8	1.9898
9		2.2483	1.5579
10		1.2927	1.4949
11		1.4687	1.569
12		1.6665	1.4894
13		1.5777	1.5459
14		1.2444	1.5926
15		1.606	1.6721
Avg		1.6367	1.5564
Stds		0.3390	0.05847

REFERENCES

- [1] M. C. Carrozza, G. Cappiello, S. Micera, B. B. Edin, L. Beccai, and C. Cipriani, "Design of a cybernetic hand for perception and action," *Bio. Cybern.*, vol. 95, no. 6, pp. 629–644, 2006.
- [2] B. B. Edin, L. Beccai, L. Ascari, S. Roccella, J.-J. Cabibihan, and M. C. Carrozza, "A bio-inspired approach for the design and characterization of a tactile sensory system for a cybernetic prosthetic hand," in *Proc. 2006 IEEE Int. Conf. Robot. Autom.*, pp. 1354–1358.
- [3] M. H. Lee and H. R. Nicholls, "Tactile sensing for mechatronics: A state of the art survey," *Mechatronics*, vol. 9, pp. 1–31, 1999.
- [4] J. Tegin and J. Wikander, "Tactile sensing in intelligent robotic manipulation: A review," *Ind. Robot: Int. J.*, vol. 32, no. 1, pp. 64–70, 2005.
- [5] D. Yamada, T. Maeno, and Y. Yamada, "Artificial finger skin having ridges and distributed tactile sensors used for grasp force control," in *Proc. RSJ/IEEE Int. Conf. Intell. Robots Syst.*, 2001, pp. 686–691.
- [6] Y. Yamada, T. Maeno, I. Fujimoto, T. Morizono, and Y. Umetani, "Identification of incipient slip phenomena based on the circuit output signals of PVDF film strips embedded in artificial finger ridges," in *Proc. SICE Annu. Conf.*, 2002, pp. 3272–3327.
- [7] B. Choi, H. R. Choi, and S. Kang, "Development of tactile sensor for detecting contact force and slip," in *Proc. 2005 IEEE/RSJ Int. Conf. Intell. Robots Syst.*, pp. 2638–2643.
- [8] A. Mingrino, A. Bucci, R. Magni, and P. Dari, "Slippage control in hand prostheses by sensing grasping forces and sliding motion," in *Proc. 1994 IEEE/RSJ/IGI Int. Conf. Intell. Robot. Syst.*, vol. 3, pp. 1803–1809.
- [9] P. Dario, R. Lazzarini, R. Magni, and S. R. Oh, "An integrated miniature fingertip sensor," in *Proc. 1996 IEEE Int. Symp. Micro Mach. Human Sci.*, pp. 91–97.
- [10] A. Cranny, D. P. J. Cotton, P. H. Chappel, S. P. Beeby, and N. M. White, "Thick-Film force and slip sensors for a prosthetic hand," *Sens. Actuators A*, vol. 123–124, pp. 162–171, 2005.
- [11] S. Sokhanvar, M. Packirisamy, and J. Daraghi, "A multifunctional PVDF-based tactile sensor for minimally invasive surgery," *Smart Mater. Struct.*, vol. 16, pp. 989–998, 2007.
- [12] K. Hosoda, Y. Tada, and M. Asada, "Anthropomorphic robotic soft fingertip with randomly distributed receptors," *Robot. Auton. Syst.*, vol. 54, pp. 104–109, 2006.
- [13] Z. Chu, P. M. Sarro, and S. Middelhoek, "Silicon three-axial tactile sensor," *Sens. Actuators A*, vol. 54, pp. 505–510, 1996.
- [14] M. Leineweber, G. Pelz, M. Schmidt, H. Kappert, and G. Zimmer, "New tactile sensor chip with silicone rubber cover," *Sens. Actuators A*, vol. 84, pp. 236–245, 2000.
- [15] T. Mei, W. J. Li, Y. Ge, Y. Chen, L. Ni, and M. H. Chan, "An integrated MEMS three-dimensional tactile sensor with large force range," *Sens. Actuators A*, vol. 80, pp. 155–162, 2000.
- [16] L. Wang and J. D. Beebe, "A silicon-based shear force sensor: Development and characterization," *Sens. Actuators A*, vol. 84, pp. 33–44, 2000.
- [17] B. J. Kane, M. A. Cutkosky, and G. T. A. Kovacs, "A traction stress sensor array for use in high-resolution robotic tactile imaging," *J. Microelectromech. Syst.*, vol. 9, no. 4, pp. 425–433, 2000.
- [18] M. Shikida, T. Shimizu, K. Sato, and K. Itoigawa, "Active tactile sensor for detecting contact force and hardness of an object," *Sens. Actuators A*, vol. 103, pp. 213–218, 2003.
- [19] Z. Wen, Y. Wu, Z. Zhang, S. Xu, S. Huang, and Y. Li, "Development of an integrated vacuum microelectronic tactile sensor array," *Sens. Actuators A*, vol. 103, pp. 301–306, 2003.
- [20] J. H. Shan, T. Mei, L. Sun, D. Y. Kong, Z. Y. Zhang, L. Ni, M. Meng, and J. R. Chu, "The design and fabrication of a flexible three-dimensional force sensor skin," in *Proc. IEEE/RSJ Int. Conf. Intell. Robots Syst. (IROS 2005)*, pp. 1965–1970.
- [21] J. Engel, J. Chen, Z. Fan, and C. Liu, "Polymer micromachined multimodal tactile sensors," *Sens. Actuators A*, vol. 117, pp. 50–61, 2005.
- [22] J. Kim, J. Lee, H. Lee, Y. Park, M. Kim, and D. Kang, "Design of flexible tactile sensor based on three-component force and its fabrication," in *Proc. 2005 IEEE Int. Conf. Robot. Autom.*, pp. 2578–2581.
- [23] E. Hwang, J. Seo, and Y. Kim, "A polymer-based flexible tactile sensor for both normal and shear load detections and its application for robotics," *J. Micromech. Syst.*, vol. 16, no. 3, pp. 784–787, 2007.
- [24] W. Cho, K. Kim, K. R. Lee, Y. Kim, D. Lee, W. H. Kim, N. Cho, K. Park, H. Park, J. Park, and B. Ju, "Flexible tactile sensor fabricated using polymer membrane," in *Proc. IEEE Sensors*, 2006, pp. 730–733.
- [25] L. Beccai, S. Roccella, A. Arena, F. Valvo, P. Valdastri, A. Menciassi, M. C. Carrozza, and P. Dario, "Design and fabrication of a hybrid silicon three-axial force sensor for biomechanical applications," *Sens. Actuators A*, vol. 120, pp. 370–382, 2005.
- [26] P. Valdastri, S. Roccella, L. Beccai, E. Cattin, A. Menciassi, M. C. Carrozza, and P. Dario, "Characterization of a novel hybrid silicon three-axial force sensor," *Sens. Actuators A*, vol. 123–124, pp. 249–257, 2005.
- [27] G. Westling and R. S. Johansson, "Responses in glabrous skin mechanoreceptors during precision grip in humans," *Exp. Brain Res.*, vol. 66, pp. 128–140, 1987.
- [28] R. S. Johansson and G. Westling, "Signals in tactile afferents from the fingers eliciting adaptive motor responses during precision grip," *Exp. Brain Res.*, vol. 66, pp. 141–154, 1987.
- [29] R. S. Johansson and B. B. Edin, "Predictive feedforward sensory control during grasping and manipulation in man," *Biomed. Res.*, vol. 14, pp. 95–106, 1993.
- [30] J.-J. Cabibihan, S. Pattofatto, M. Jomaa, A. Benallal, M. C. Carrozza, and P. Dario, "The conformance test for robotic/prosthetic fingertip skins," in *Proc. 1st IEEE/RAS-EMBS Int. Conf. Biomed. Robot. Biomech.*, 2006, pp. 561–566.
- [31] E. R. Kandel, J. H. Schwartz, and T. M. Jessell, *Principles of Neural Science*, 4th ed. New York: McGraw-Hill, 2000.
- [32] M. Basseville and A. Benveniste, "Design and comparative study of some sequential jump detection algorithms for digital signals," *IEEE Trans. Acoust., Speech, Signal Process.*, vol. 31, no. 3, pp. 521–535, Jan. 1983.
- [33] B. B. Edin, L. Ascari, L. Beccai, S. Roccella, J.-J. Cabibihan, and M. C. Carrozza, "Bio-inspired sensorization of a biomechatronic robot hand for the grasp-and-lift tasks," *Brain Res. Bull.*, vol. 75, pp. 785–795, 2008.
- [34] M. C. Carrozza, C. Suppo, F. Sebastiani, B. Massa, F. Vecchi, R. Lazzarini, M. R. Cutkosky, and P. Dario, "The SPRING hand: Development of a self-adaptive prosthesis for restoring natural grasping," *Auton. Robots*, vol. 16, no. 2, pp. 125–141, 2004.
- [35] B. Massa, S. Roccella, M. C. Carrozza, and P. Dario, "Design and development of an underactuated prosthetic hand," in *Proc. 2002 IEEE Int. Conf. Robot. Autom.*, vol. 4, pp. 3374–3379.
- [36] M. C. Carrozza, G. Cappiello, L. Beccai, F. Zaccone, S. Micera, and P. Dario, "Design methods for innovative hand prostheses," in *Proc. 26th Annu. Int. Conf. Eng. Med. Biol. Soc.*, 2004, vol. 6, pp. 4345–4348.



Lucia Beccai (M'06) received the Laurea degree in electronic engineering from the University of Pisa, Pisa, Italy, in 1998, and the Ph.D. degree in microsystem engineering from the University of Rome Tor Vergata, Rome, Italy, in 2003.

In 1999, she joined the Center of Research in Microengineering (CRIM) Laboratory, Scuola Superiore Sant'Anna, Anna, where she was engaged with European Scientific Projects in the field of biomedical microsystems for physiological parameters monitoring and sensory systems for human machine interfaces. From 2002 to 2005, she was a Project Manager of the CYBERHAND Project (EU-IST-FET-2001-35094 <http://www.cyberhand.org>), and involved to the development of the tactile sensory system of the artificial hand. She is currently a Research Scientist at the Advanced Robotic Technology and System (ARTS) Laboratory, Scuola Superiore Sant'Anna, from December 2005. She is currently involved in several international projects. Her current research interests include biomechanics and microsystems design for investigation of bio-inspired sensory systems for artificial hands, and development of hand prosthesis sensory tactile feedback systems.



Stefano Roccella received the Laurea degree in aeronautical engineering from the University of Pisa, Pisa, Italy, in 1999. He is working toward the Ph.D. degree in robotics at the University of Genova, Genova, Italy.

In 1999, he joined the Advanced Robotic Technology and System (ARTS) Laboratory, Scuola Superiore Sant'Anna, Ann, as a Research Assistant. He is currently an Assistant Professor of Biomedical Robotics at Scuola Sant'Anna, where he is member of the ARTS Lab. His current research interests include biomedical robotics, rehabilitation engineering, biomechanics, and micro-electro-mechanical systems (MEMS) design and development.

Mr. Rocella is a member of the ARTS Laboratory.



Luca Ascari (S'99–M'05) received the Laurea degree in electrical engineering from the University of Parma, Parma, Italy, in 2000, and the Ph.D. degree (with honours) in bioengineering from the Scuola Superiore Sant'Anna, Anna, Italy, in 2005.

In 2000, he was with Philips Research Laboratories, In 2001, he was with Marconi Photonics Research Laboratories. In 2002, he joined Center of Research in Microengineering (CRIM) Laboratories, Scuola Superiore Sant'Anna where he worked in several public and private-funded international research projects. Since 2005, he has been a Visiting Scientist at Pazmany University, Budapest, Hungary and Analogic and Neural Computing Laboratory, at Forschungszentrum Informatik (FZI), Karlsruhe, Germany, and at Department of Integrative Medical Biology, Physiology Section, Umeå University, Sweden. He is currently a Research Fellow at Centre of Excellence for Information and Communication Engineering (CEIIC) of the Scuola Superiore Sant'Anna. He is the author or coauthor of more than 20 scientific papers and three European patents. His current research interests include biophotonics, artificial multimodal perception systems for robotics, and neuromorphic computation. He is a Co-Founder of HENESIS s.r.l., a spin-off company of the Scuola Superiore Sant'Anna, where he has been the President and CEO since 2007.

Dr. Ascari is a member of the IEEE Robotics and Automation Society (RAS).



Pietro Valdastri (M'05) received the Laurea degree (with honors) in electronic engineering from the University of Pisa, Pisa, Italy, in 2002, and the Ph.D. degree in bioengineering from the Center of Research In Microengineering (CRIM) Laboratory, Scuola Superiore Sant'Anna, Pisa, in 2006.

He is currently a Postdoctoral Fellow at the CRIM Laboratory. His current research interests include the field of implantable robotic systems and active capsular endoscopy. He is also working on several European projects for the development of minimally invasive and wireless biomedical devices.



Arne Sieber (M'06) received the degree in biomedical engineering from the Technical University of Graz, Graz, Austria, in 1999, and the Ph.D. degree in electrochemical sensors in 2002.

From 1997 to 2001, he was at AVL Medical Instruments, Graz. The next four years he worked for Roche Diagnostics in the R&D of electrochemical and optical sensors. He is currently a Researcher in the R&D of Microsensors and Actuators, Profactor Research and Solutions GmbH, Seibersdorf, Austria. Within a knowledge transfer program, he has also been part of a research team for the last year at the Center of Research In Microengineering (CRIM) Laboratory, Scuola Superiore Sant'Anna, Pisa, Italy.



M. Chiara Carrozza (M'00) received the Laurea degree in physics from the University of Pisa, Pisa, Italy, in 1990, and the Ph.D. degree in engineering from the Scuola Superiore Sant'Anna, Pisa, in 1994.

Since 2001, she has been an Associate Professor of biomedical robotics at the Scuola Superiore Sant'Anna, where she is the Deputy Director, and also the Director of the Research Division. She is a cofounder of two spin-off of the Scuola Superiore Sant'Anna and is a member of their Administrative Boards. She also teaches biomechanics and rehabilitation engineering at the University of Pisa. She was a Visiting Professor at the Technical University of Wien, Austria, with a graduate course entitled Biomechanics. She is involved in the scientific management of the Italy–Japan joint laboratory for Humanoid Robotics ROBOCASA, Waseda University, Tokyo, Japan, where she is responsible for artificial hand design. She is also the Coordinator of the Advanced Robotics Technology and Systems Laboratory. She is active in several national and international projects in the fields of biomechanics and biomedical robotics. Her current research interests include biomedical robotics (cybernetic and robotic artificial hands, upper limb exoskeletons), rehabilitation engineering (neuro-rehabilitation, domotic, and robotic aids for functional support and personal assistance), and biomedical microengineering (microsensors, tactile sensors). She coordinated the Arts Laboratory and designed and developed the CYBERHAND artificial hand. She is currently responsible for the design of an exoskeleton for functional support and enhancement of the upper limb, in the framework of the NEUROBOTICS project. She is the author or coauthor of several scientific papers and international patents. In addition, she is promoting industrial innovation and start-up creation.

Prof. Carrozza is an elected Member of the National Board of the Italian Association of Biomedical Engineering (Gruppo Nazionale di Bioingegneria). She is a Member of the IEEE Robotics and Automation Society (RAS) and the IEEE Engineering in Medicine and Biology Society (EMBS).



Paolo Dario (M'99–SM'01–F'03) received the Dr. Eng. Degree in mechanical engineering from the University of Pisa, Pisa, Italy, in 1977.

He is a full Professor of biomedical robotics at the Scuola Superiore Sant'Anna, Pisa, where he is also the Director of Polo Sant'Anna Valdera and the Center of Research in Microengineering (CRIM) Laboratory, where he supervises a team of about 70 researchers. He has been a Visiting Professor at the Ecole Polytechnique Federale de Lausanne (EPFL), Switzerland, and at Waseda University, Tokyo, Japan. His current research interests include the fields of biorobotics, biomedical engineering, biomechanics, and microengineering. He is the coordinator of many national and European projects, the editor of four books on the subject of robotics, and the author or coauthor of more than 200 scientific papers.

Prof. Dario was the President of the IEEE Robotics and Automation Society in 2001–2002. He is an Associate Editor of the IEEE TRANSACTIONS ON ROBOTICS AND AUTOMATION. He is also the Co-Chair of the Technical Committees on Biorobotics and Robo-Ethics.